In situ high-pressure synchrotron x-ray diffraction study of $Zr_2(WO_4)(PO_4)_2$ up to 16 GPa

Mehmet Cetinkol and Angus P. Wilkinson*
School of Chemistry and Biochemistry, Georgia Institute of Technology, Atlanta, Georgia 30332-0400, USA

Cora Lind
Department of Chemistry, The University of Toledo, Toledo, Ohio 43606-3390, USA

(Received 25 September 2008; revised manuscript received 15 May 2009; published 29 June 2009)

The negative thermal-expansion material $Zr_2(WO_4)(PO_4)_2$ adopts the orthorhombic $Sc_2(WO_4)_3$ structure under ambient conditions. Synchrotron x-ray powder diffraction was used to study its behavior on compression in a diamond-anvil cell up to 16 GPa. Three crystalline-to-crystalline phase transitions were observed. The material was orthorhombic (*Pnca*) in the pressure range 0.0–1.37 GPa, monoclinic between 1.68 and 3.7 GPa, monoclinic with a different structure between 3.7 and 6.3 GPa, and triclinic between 7.4 and 14 GPa. Bulk moduli for these phases were estimated using a Birch-Murnaghan equation of state to be 49(2), 17(1), 37(1), and 76(7) GPa, respectively. The first two phase transitions were reversible on decompression. Irreversible partial amorphization was observed above 14 GPa. This sequence of phase transitions, and the pressure at which the first transition occurs, is significantly different from that previously observed for $A_2(MO_4)_3$ (*A* is any +3 ion, *M* is Mo or W) compounds that adopt a $Sc_2(WO_4)_3$ structure under ambient conditions.

DOI: 10.1103/PhysRevB.79.224118 PACS number(s): 61.50.Ks, 62.50.−p, 62.20.−x

I. INTRODUCTION

Oxides exhibiting low and negative thermal expansion (NTE) have been of considerable recent interest,[1–7] with many of them belonging to one of the following structural families: NZP-type,[8–12] ZrW_2O_8-type,[13–15] ZrV_2O_7-type,[16] and $Sc_2(WO_4)_3$-type.[7] Such materials may find application as pure phases or in controlled thermal-expansion composites.[17–20] Many NTE compounds have been shown to undergo crystalline-to-crystalline phase transitions,[13,21–24] and/or pressure-induced amorphization[15,21,25–28] upon application of modest pressures. During their manufacture and use, pressures above ambient may be encountered leading to phase transitions and a loss of, or change in, NTE.[29,30] As a consequence, high-pressure studies of NTE materials are of some importance from a practical standpoint as well as being of fundamental interest.

$A_2(MO_4)_3$ (*A*=many 3+ions, *M*=Mo or W) compounds are known to adopt a variety of different structures depending upon the nature of A^{3+}.[31–34] The orthorhombic $Sc_2(WO_4)_3$ structure (*Pnca*), which is often associated with volume NTE, has been observed for *A*=Al, Sc, Cr, Fe, Y, In, and the smaller rare earths from Lu to Ho. With decreasing temperatures, several compounds in the $Sc_2(WO_4)_3$ family display a ferroelastic phase transition to a monoclinic ($P2_1/a$) structure, which does not exhibit NTE.[34–36] The temperature for this transition has been proposed to be dependent on the electronegativity of the A^{3+} cation.[34] Several members of the $Sc_2(WO_4)_3$ structural family have been studied under pressure and were reported to display a variety of crystalline-to-crystalline phase transitions and pressure-induced amorphization.[24,28,37–41]

Additional structural relatives of $Sc_2(WO_4)_3$ can be prepared by substitution on the scandium and/or tungsten sites. The possibilities include trivial substitutions, for example, $(ScAl)(WO_4)_3$ and $(ErIn)(WO_4)_3$,[7] as well as more complicated ones such as $(HfMg)(WO_4)_3$,[42,43] $Zr_2WO_4(PO_4)_2$,[44–46] $Zr_2MoO_4(PO_4)_2$,[47] and the Hf analogs of these phosphates.[7] The effect of the more complex substitutions on the high-pressure behavior of this structure type is unknown.

In this paper, we present a high-pressure *in situ* monochromatic synchrotron powder-diffraction study of $Zr_2(WO_4)(PO_4)_2$ at room temperature in a diamond-anvil cell and compare its behavior to that of other $Sc_2(WO_4)_3$ type materials. The existence of $Zr_2(WO_4)(PO_4)_2$ was first described by Martinek and Hummel[44] in 1970. Evans *et al.*[46] reported its crystal structure (*Pnca*) as belonging to the $Sc_2(WO_4)_3$ structural family and comprised of ZrO_6 octahedra sharing corners with WO_4 and PO_4 tetrahedra. Its mean linear coefficient of thermal expansion has previously been reported as -6×10^{-6} and -3×10^{-6} K^{-1} based on dilatometeric and x-ray diffraction measurements, respectively.[7] Very recent variable-temperature neutron measurements indicate $\alpha_v=-14.0(10)\times10^{-6}$ K^{-1}, $\alpha_a=-7.9(5)\times10^{-6}$ K^{-1}, $\alpha_b=2.5(5)\times10^{-6}$ K^{-1}, and $\alpha_c=-8.7(2)\times10^{-6}$ K^{-1} over the range 60–300 K.[48]

II. EXPERIMENTAL

A. Sample preparation

$Zr_2(WO_4)(PO_4)_2$ was prepared using a literature method.[46] Stoichiometric amounts of ZrO_2 (Alfa Aesar, 99.7%), WO_3 (Strem Chemicals, 99.8 %), and ZrP_2O_7 were ground together in an agate mortar, heated in a Pt crucible for 5 h at 900 °C followed by 8 h at 1250 °C in air. ZrP_2O_7 was prepared by heating stoichiometric amounts of dehydrated $ZrO(NO_3)_2\cdot xH_2O$ (Alfa Aesar) and $(NH_4)_2HPO_4$ (J.T. Baker, 99.2%) for 20 h at 700 °C in a Pt crucible.

B. Diamond-anvil cell and diffraction data collection

High-pressure *in situ* powder-diffraction data were collected at room temperature using the B-2 line of the Cornell High Energy Synchrotron Source (CHESS), Wilson Lab, Cornell University, Ithaca, NY. Data were obtained from two

separate runs using a four-post diamond-anvil cell (DAC) with a methanol-ethanol (4:1) pressure medium. The DAC had 2.1-mm-thick diamonds with 600 μm culet faces. A pre-indented fully hardened stainless-steel gasket with 250 μm initial thickness and a 150 μm diameter hole was used. This pressure transmitting medium is claimed to be hydrostatic up to 10.4 GPa.[49] For both runs, x rays of wavelength 0.4960(5) Å were selected using a Ge(111) double-crystal monochromator and the beam collimated with a ~50 μm pin hole. Diffraction patterns were recorded on a Mar345 imaging plate detector. The sample-to-detector distance was calibrated using ambient pressure diffraction from a TaO_2F sample in a previous experiment.[50] Pressure was determined using the ruby fluorescence technique.[51]

For the first run, the initial pressure was ambient and 23 diffraction patterns were collected up to 5.35 GPa on compression and 21 patterns were collected during decompression to 0.08 GPa. For the second set of measurements, the starting pressure was 0.44 GPa and 18 patterns were collected up to 16 GPa and the cell was decompressed to ~1.4 GPa in four large steps.

C. Data processing

The two-dimensional diffraction images were integrated using the program FIT2D.[52] $I(2\theta)$ data were initially processed in JADE.[53] The high-pressure phases were indexed with TREOR (Ref. 54) implemented in the program CMPR (Ref. 55) and then further analyzed using the GSAS program suite[56] with the EXPGUI (Ref. 57) interface. The calculated unit-cell volumes were fitted to a Birch-Murnaghan equation of state (EoS) (Ref. 58) using the EOS-FIT program (v5.2).[59]

III. RESULTS

Two reversible crystalline-to-crystalline phase transitions are apparent from the data shown in Fig. 1. The Bragg peaks at ~3.8° and ~6.4° 2θ get broader and then split during the first transition. The absence of broadening in the peak at ~4.6° 2θ provides assurance that the broadening of the other peaks is not due to the loss of hydrostatic conditions. The transition onset pressure, as indicated by an examination of the full width at half maximum for the peaks at ~3.8° and ~6.4° 2θ as a function of pressure (Fig. 2) during compression is ~1.4 GPa. This new phase was indexed as monoclinic, possible space group $P2_1/n11$, using TREOR.

When the pressure was increased above 3.41 GPa, another phase formed as indicated by the emergence of new peaks. This second transition is most likely discontinuous, as two phases seem to coexist over a narrow range of pressures. This phase was also indexed as monoclinic, probable space group $P2_1/n11$. Both transitions were reversible on decompression. Lattice constants from Le Bail fits to each diffraction pattern from this run are given in Table I. Unit-cell volume as a function of pressure is shown in Fig. 3. The normalized unit-cell volumes on compression and decompression are in agreement between 3.5 and 5.5 GPa, but the values below 3.5 GPa appear to be slightly different from one another. This could be a consequence of an experimental

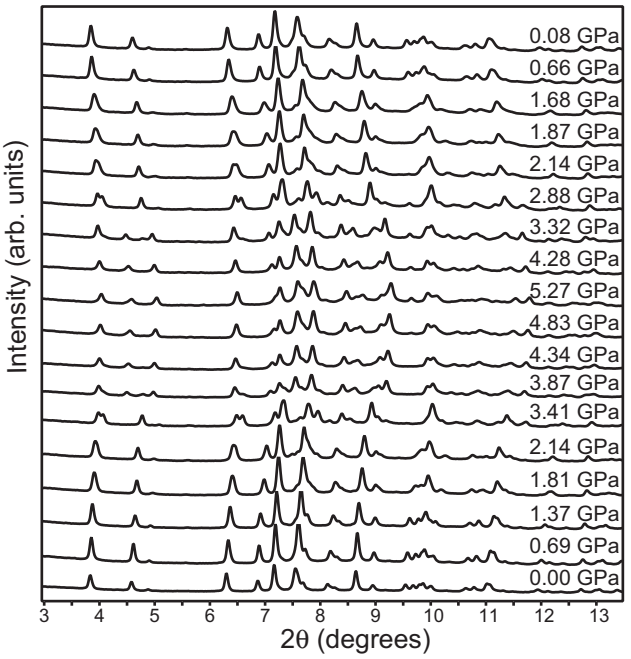

FIG. 1. Selected diffraction patterns for $Zr_2(WO_4)(PO_4)_2$ on compression to 5.27 GPa followed by decompression (experimental run 1). Phase transitions occur at ~1.4 and ~3.7 GPa. These changes are reversible on decompression.

error, such as the sample-to-image plate distance changing during our experiment, or to hysteresis. An examination of the individual lattice constants on compression and decompression (Figs. 4 and 5) indicates that the observed phenomenon is not due to a change in sample-to-plate distance or any similar experimental error, as some of the lattice constants change in a reversible way on compression and decompression, but others do not.

For the second run (Fig. 6), the pressure range was more extensive than in the first, and three crystalline-to-crystalline phase transitions were seen along with a disordering, or par-

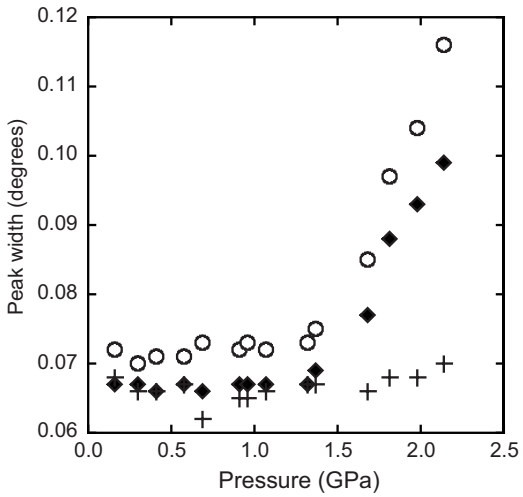

FIG. 2. Full width at half maximum for the Bragg peaks located at ~3.8° (filled diamonds), ~4.6° (crosses), and ~6.4° (open circles) 2θ in the data shown in Fig. 1. Their pressure dependence indicates a phase transition at ~1.4 GPa.

TABLE I. $Zr_2(WO_4)(PO_4)_2$ lattice constants and unit-cell volume as a function of pressure determined by Le Bail fits to the diffraction patterns from experimental run 1. Uncertainties in the pressures are expected to be 0.05–0.1 GPa.

P (GPa)	Phase	*a* (Å)	*b* (Å)	*c* (Å)	α (deg)	Volume (Å^3)
0.00	Ortho	9.3543(3)	12.3288(5)	9.1708(4)		1057.65(5)
0.16	Ortho	9.3507(3)	12.3107(5)	9.1656(4)		1055.08(5)
0.30	Ortho	9.3462(4)	12.2911(5)	9.1566(4)		1051.87(5)
0.41	Ortho	9.3419(4)	12.2780(5)	9.1517(4)		1049.70(5)
0.58	Ortho	9.3363(3)	12.2558(4)	9.1422(4)		1046.09(5)
0.69	Ortho	9.3326(3)	12.2342(4)	9.1365(4)		1043.18(5)
0.91	Ortho	9.3265(4)	12.2106(6)	9.1273(5)		1039.44(6)
0.96	Ortho	9.3242(4)	12.1983(5)	9.1211(5)		1037.43(6)
1.07	Ortho	9.3232(4)	12.1909(5)	9.1189(5)		1036.44(6)
1.32	Ortho	9.3174(4)	12.1743(6)	9.1102(5)		1033.40(6)
1.37	Ortho	9.3101(3)	12.1540(8)	9.1003(6)		1029.74(7)
1.68	Mono 1	9.2959(6)	12.0950(8)	9.0466(8)	89.60(1)	1017.13(8)
1.81	Mono 1	9.2935(5)	12.0699(8)	8.9978(5)	89.495(7)	1009.26(7)
1.98	Mono 1	9.2872(6)	12.049(1)	8.9716(7)	89.398(7)	1003.86(8)
2.14	Mono 1	9.2818(6)	12.0199(9)	8.9308(7)	89.306(8)	996.30(8)
2.55	Mono 1	9.2738(3)	11.9633(6)	8.8597(5)	89.149(5)	982.83(6)
2.80	Mono 1	9.2712(6)	11.9253(8)	8.8131(8)	89.089(7)	974.27(8)
2.99	Mono 1	9.2642(7)	11.876(1)	8.7596(7)	88.897(1)	963.58(8)
3.41	Mono 1	9.2595(4)	11.8297(6)	8.7057(5)	88.646(5)	953.33(5)
3.87	Mono 1	9.238(2)	11.828(2)	8.701(2)	88.39(2)	950.4(2)
	Mono 2	9.3473(8)	11.4280(7)	8.2372(7)	97.261(7)	872.84(7)
4.34	Mono 2	9.3371(6)	11.3967(6)	8.2095(5)	97.374(5)	866.37(5)
4.83	Mono 2	9.3403(8)	11.3549(8)	8.1760(8)	97.443(8)	859.83(8)
5.14	Mono 2	9.3539(8)	11.3243(7)	8.1302(8)	97.621(7)	853.60(8)
5.35	Mono 2	9.3694(9)	11.2988(9)	8.0931(9)	97.672(8)	849.09(8)
5.27	Mono 2	9.3693(8)	11.3157(7)	8.0985(8)	97.616(6)	851.03(8)
5.03	Mono 2	9.3649(8)	11.3283(8)	8.1153(9)	97.579(7)	853.42(9)
4.81	Mono 2	9.3566(7)	11.3522(7)	8.1393(9)	97.554(6)	857.03(8)
4.75	Mono 2	9.3540(7)	11.3573(7)	8.1557(7)	97.546(6)	858.93(7)
4.56	Mono 2	9.3489(7)	11.3694(8)	8.1729(6)	97.506(6)	861.28(6)
4.39	Mono 2	9.3465(7)	11.3845(7)	8.1931(6)	97.424(6)	864.49(6)
4.28	Mono 2	9.3455(7)	11.4024(7)	8.2086(6)	97.370(6)	867.49(6)
4.01	Mono 2	9.3466(5)	11.4217(5)	8.2289(5)	97.310(5)	871.33(5)
3.46	Mono 2	9.3403(8)	11.4679(7)	8.2734(7)	97.216(7)	879.17(7)
3.32	Mono 2	9.3388(6)	11.4824(6)	8.2944(5)	97.254(6)	882.31(6)
	Mono 1	9.2766(7)	11.8291(8)	8.6883(9)	88.652(8)	953.1(1)
2.88	Mono 1	9.2773(6)	11.8649(8)	8.7421(6)	88.649(8)	962.01(7)
2.64	Mono 1	9.2774(6)	11.8985(9)	8.7778(7)	88.83(1)	968.76(8)
2.28	Mono 1	9.2762(5)	11.9511(9)	8.8324(7)	89.051(8)	979.03(8)
2.14	Mono 1	9.2884(5)	11.9824(7)	8.8685(6)	89.122(6)	986.92(7)
1.87	Mono 1	9.2933(5)	12.0196(8)	8.9194(6)	89.228(7)	996.22(8)
1.68	Mono 1	9.3054(5)	12.0718(9)	8.9899(7)	89.417(8)	1009.81(9)
1.02	Ortho	9.3188(6)	12.1707(8)	9.1001(8)		1032.10(9)
0.66	Ortho	9.3334(7)	12.2111(8)	9.1222(8)		1039.67(9)
0.44	Ortho	9.3392(7)	12.2397(9)	9.1330(8)		1043.98(9)
0.16	Ortho	9.3476(7)	12.281(1)	9.1488(8)		1050.3(1)
0.08	Ortho	9.3428(7)	12.2855(9)	9.1490(8)		1050.13(9)

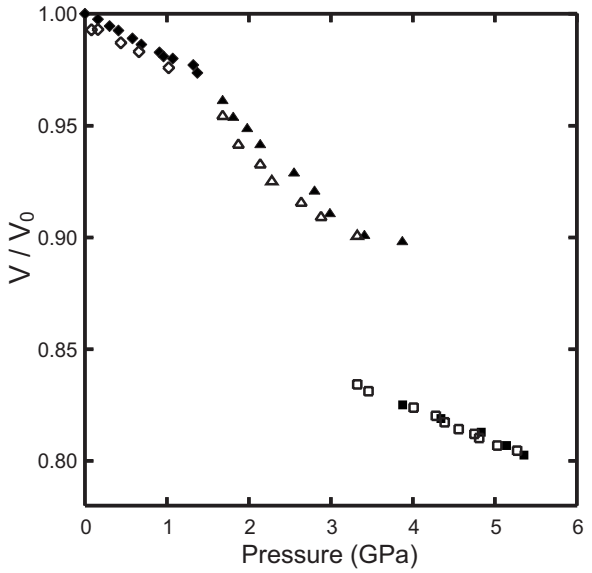

FIG. 3. Normalized unit-cell volumes from experimental run 1 for $Zr_2(WO_4)(PO_4)_2$. Closed symbols are values on compression and open symbols are on decompression.

tial amorphization, above 14 GPa. The disordering was not reversible and remnant Bragg peaks suggestive of the highest pressure crystalline phase persisted on decompression. The diffraction patterns from this run could be indexed on an orthorhombic unit cell (*Pnca*) for pressures up to 1.2 GPa. At the next pressure point (1.94 GPa), the pattern could be indexed as monoclinic. A transition leading to a second monoclinic phase was observed between 2.97 and 3.70 GPa. In the pressure range 5.66–9.94 GPa the behavior of the second Bragg peak in the diffraction pattern suggests another crystalline-to-crystalline phase transition with some phase

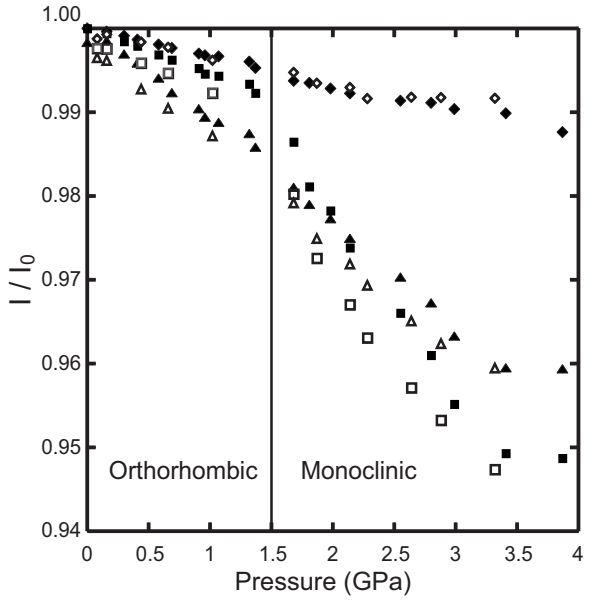

FIG. 4. Normalized unit-cell constants for $Zr_2(WO_4)(PO_4)_2$ from experimental run 1. Filled symbols are values determined on compression and open symbols are on decompression. *a*-axis diamonds; *b*-axis triangles; *c*-axis squares.

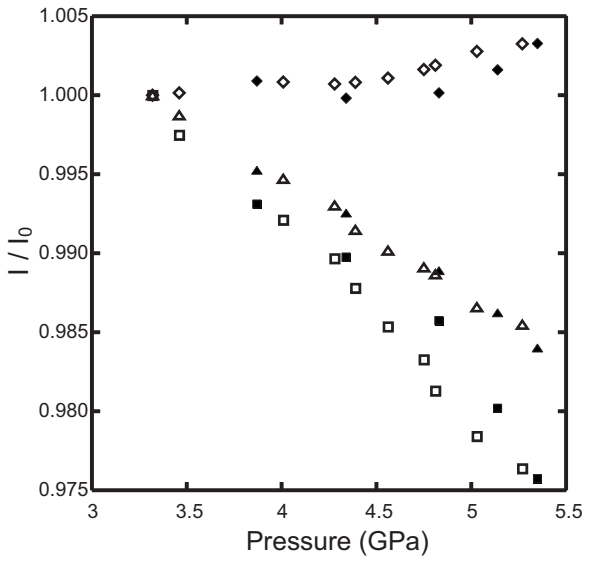

FIG. 5. Normalized unit-cell constants for the second monoclinic phase of $Zr_2(WO_4)(PO_4)_2$ from run 1. Filled symbols are values determined on compression and open symbols are on decompression. *a*-axis diamonds; *b*-axis triangles; *c*-axis squares.

coexistence. This is followed by partial amorphization above 14 GPa. The highest pressure crystalline phase was indexed on a triclinic unit cell using TREOR (Ref. 54) implemented in the program CMPR.[55] Lattice constants derived from the Le Bail fits to the data from run 2 are given in Table II. Normalized unit-cell volumes from runs 1 and 2 on compression are compared in Fig. 7. The agreement between the two sets of measurements is not ideal, perhaps in part reflecting dif-

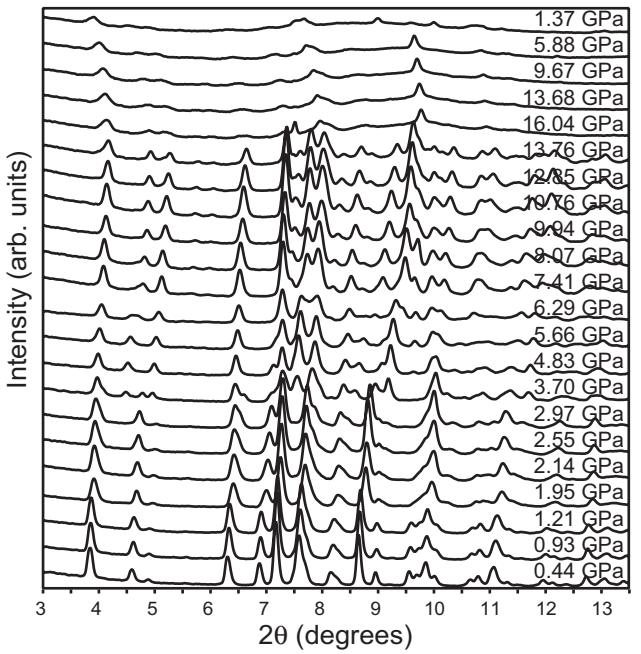

FIG. 6. Selected diffraction patterns for $Zr_2(WO_4)(PO_4)_2$ on compression to ~16 GPa followed by decompression. In addition to the phase transitions seen in the earlier run, another transition is observed at 7.4 GPa. The partial amorphization seen at >14 GPa is not reversible on decompression.

TABLE II. $Zr_2(WO_4)(PO_4)_2$ lattice constants and unit-cell volume as a function of pressure determined by Le Bail fits to the diffraction patterns obtained on compression during run 2. As the observed high-pressure disordering did not reverse on decompression, lattice constants could not be determined for decompression. Uncertainties in the pressures are expected to be 0.05–0.1 GPa.

P (GPa)	Phase	*a* (Å)	*b* (Å)	*c* (Å)	α (deg)	β (deg)	γ (deg)	Volume (Å^3)
0.44	Ortho	9.3479(6)	12.292(1)	9.1608(7)				1052.6(1)
0.93	Ortho	9.3294(6)	12.2345(8)	9.1304(7)				1042.14(9)
1.21	Ortho	9.3226(6)	12.2069(9)	9.1135(7)				1037.11(9)
1.95	Mono 1	9.2719(7)	12.107(1)	8.9766(9)	89.56(1)			1007.7(1)
2.14	Mono 1	9.2775(7)	12.037(1)	8.9375(8)	89.27(1)			998.0(1)
2.55	Mono 1	9.2747(8)	11.9952(2)	8.8960(8)	89.12(1)			989.6(1)
2.97	Mono 1	9.2774(7)	11.9503(2)	8.8335(7)	88.95(1)			979.2(1)
3.70	Mono 1	9.239(1)	11.8474(2)	8.712(1)	88.45(2)			953.2(1)
	Mono 2	9.301(1)	11.467(1)	8.259(1)	97.289(8)			873.7(1)
4.83	Mono 2	9.2925(7)	11.4186(8)	8.2383(6)	97.392(7)			866.88(7)
5.66	Mono 2	9.3130(6)	11.3435(8)	8.1571(8)	97.593(7)			854.18(6)
6.29	Mono 2	9.355(1)	11.301(1)	8.116(1)	97.78(1)			850.1(1)
	Tric	11.204(2)	9.374(2)	12.499(2)	88.229(8)	141.717(5)	91.43(2)	812.9(2)
7.41	Tric	11.1475(8)	9.3759(7)	12.515(1)	88.866(4)	141.654(2)	90.930(7)	811.34(7)
8.07	Tric	11.1388(7)	9.389(1)	12.464(1)	88.875(5)	141.622(2)	90.947(8)	809.15(9)
9.94	Tric	11.0392(9)	9.370(1)	12.408(1)	89.280(5)	141.610(2)	90.591(9)	796.97(8)
10.76	Tric	10.996(1)	9.377(1)	12.363(1)	89.209(5)	141.495(3)	90.67(2)	793.64(8)
12.85	Tric	10.9258(6)	9.3460(6)	12.2423(7)	89.472(3)	141.641(2)	90.420(5)	775.76(2)
13.76	Tric	10.877(1)	9.3407(9)	12.196(1)	89.474(5)	141.578(3)	90.40(1)	770.02(6)

ferent sample-to-detector calibration errors for the two runs. As more extensive data are available at low pressure from run 1, this run is the basis of most subsequent discussion for pressures below 6 GPa.

Normalized lattice constants for phases 1 and 2 are shown in Fig. 4. There appear to be no discontinuities in the lattice constants at the first phase transition, suggestive of second-order behavior. Both phases are anisotropically compressible, with the second (monoclinic) phase showing much greater anisotropy. The compressibilities of the *a* and *b* axes are almost continuous through the transition, but the *c* axis softens considerably on going to the monoclinic phase. Average linear compressibilities for the initial orthorhombic phase were estimated to be $\beta_a = 3.3(1) \times 10^{-3}$ GPa^{-1}, $\beta_b = 10.3(3) \times 10^{-3}$ GPa^{-1}, and $\beta_c = 5.5(2) \times 10^{-3}$ GPa^{-1} by least-squares fits of a straight line to the lattice constants as a function of pressure. The corresponding values for the monoclinic phase existing below ~4 GPa are $\beta_a = 2.3(1) \times 10^{-3}$ GPa^{-1}, $\beta_b = 13.0(4) \times 10^{-3}$ GPa^{-1}, and $\beta_c = 22.0(8) \times 10^{-3}$ GPa^{-1}. Normalized lattice constants for the second monoclinic phase (Fig. 5) also indicate considerable anisotropy for the compressibility of this phase, with average linear compressibilities for this phase of $\beta_a = -15(10) \times 10^{-4}$ GPa^{-1}, $\beta_b = 7.6(4) \times 10^{-3}$ GPa^{-1}, and $\beta_c = 12(2) \times 10^{-3}$ GPa^{-1}. Linear compressibilities on compression and decompression are summarized in Table III.

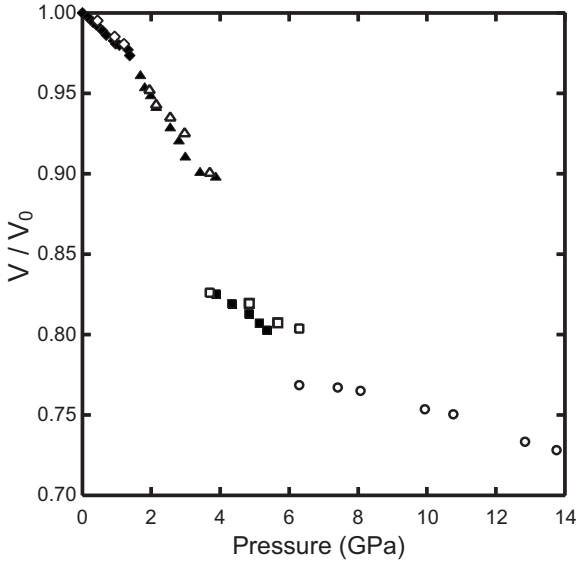

FIG. 7. Normalized unit-cell volumes for $Zr_2(WO_4)(PO_4)_2$ from experimental run 1 (closed symbols) and run 2 (open symbols) on compression only.

For all the phases observed, a third order Birch-Murnaghan EoS was fit to the *P*-*V* data shown in Tables I and II. However, data at pressures where phase coexistence was observed were in some cases excluded from these fits due to large errors in the estimated unit-cell volumes. During the fitting, it was found that the pressure derivative of the bulk modulus (K_p) was not well determined by the data, so it was fixed at 4.0 while varying the zero pressure volume (V_0) and zero pressure bulk modulus (K_0). In general, the agreement between the EoS models and the experimental observations was good, given the errors expected for the pressure

TABLE III. Linear compressibilities (β) for the different phases observed during the compression and decompression of $Zr_2(WO_4)(PO_4)_2$. The values reported were obtained from linear fits to ln(lattice constant) vs p.

		Run 1	Run 1	Run 2
Ortho	P range (GPa)	0.0–1.37	1.02–0.08	0.44–1.2
	β_a	$3.3(1)\times10^{-3}$	$3.0(5)\times10^{-3}$	$3.6(4)\times10^{-3}$
	β_b	$10.3(3)\times10^{-3}$	$10.3(4)\times10^{-3}$	$9.1(4)\times10^{-3}$
	β_c	$5.5(2)\times10^{-3}$	$5.8(3)\times10^{-3}$	$6.74(5)\times10^{-3}$
Mono 1	P range (GPa)	1.68–3.41	2.88–1.68	1.95–2.97
	β_a	$2.3(1)\times10^{-3}$	$2.4(7)\times10^{-3}$	$-0.4(4)\times10^{-3}$
	β_b	$13.0(4)\times10^{-3}$	$14.0(7)\times10^{-3}$	$12(2)\times10^{-3}$
	β_c	$22.0(8)\times10^{-3}$	$22(2)\times10^{-3}$	$15(1)\times10^{-3}$
Mono 2	P range (GPa)	3.87–5.35	5.27–3.32	3.7–6.3
	β_a	$-15(10)\times10^{-4}$	$-1.5(2)\times10^{-3}$	$-21(12)\times10^{-4}$
	β_b	$7.6(4)\times10^{-3}$	$7.6(2)\times10^{-3}$	$5.8(6)\times10^{-3}$
	β_c	$12(2)\times10^{-3}$	$12.3(4)\times10^{-3}$	$7(2)\times10^{-3}$
Triclinic	P range (GPa)			7.41–13.76
	β_a			$3.9(2)\times10^{-3}$
	β_b			$0.7(2)\times10^{-3}$
	β_c			$4.0(2)\times10^{-3}$

calibration procedure, with the exception of pressures where phase coexistence was observed. Additionally, bulk moduli averaged over the pressure range of the data were estimated using a straight-line fit to ln(V) vs p. These moduli are presented in Table IV.

IV. DISCUSSION

The behavior of $Zr_2(WO_4)(PO_4)_2$ on compression is different from that previously observed for other orthorhombic $A_2(MO_4)_3$ phases such as $Sc_2(WO_4)_3$, $Sc_2(MoO_4)_3$, $Al_2(WO_4)_3$, and $Y_2(WO_4)_3$ in several important respects. A summary of the high-pressure behavior for these compounds is presented in Table V.

The initial negative thermal-expansion orthorhombic structure (*Pnca*) for $Zr_2(WO_4)(PO_4)_2$ persists to a much higher pressure (~1.4 GPa) than was observed for $Sc_2(WO_4)_3$ (~0.3 GPa), $Sc_2(MoO_4)_3$ (~0.25 GPa), or $Al_2(WO_4)_3$ (~0.1 GPa). This is potentially significant as the transition pressure for the later group of compounds fall in the regime that could be readily reached during the processing or use of these materials. While $Y_2(WO_4)_3$ was reported not to undergo any phase transitions at low pressure,[60] it is susceptible to hydration in moist air.[64] The origins of these differences are unclear.

Orthorhombic $Zr_2(WO_4)(PO_4)_2$ has a bulk modulus, K_0 =49(2) GPa, that is greater than that for the scandium containing phases (~31 GPa) (Ref. 24) and $Y_2(WO_4)_3$ (~25 GPa),[60] but similar to that for aluminum tungstate (~48 GPa).[24] These observations are in line with the measured volumes per oxide ion for these phases: $Zr_2(WO_4)(PO_4)_2$, 22.0 Å^3; $Al_2(WO_4)_3$, 21.7 Å^3; $Sc_2(WO_4)_3$, 25.7 Å^3; $Sc_2(MoO_4)_3$, 25.4 Å^3; $Y_2(WO_4)_3$, 28.7 Å^3.

On compressing the scandium and aluminum phases,[24] they transform to the same monoclinic structure (*Pnca* $\rightarrow P2_1/a$) that occurs on cooling $Al_2(WO_4)_3$, or $Sc_2(MoO_4)_3$,[35] via a discontinuous pathway. This monoclinic structure has twice as many f.u. per primitive unit cell as the original *Pnca* phase. However, the first monoclinic structure seen on compressing $Zr_2(WO_4)(PO_4)_2$ is formed in an apparently continuous fashion. The monoclinic unit cell proposed for $Zr_2(WO_4)(PO_4)_2$ can be readily transformed to one similar to that expected for a monoclinic $Sc_2(MoO_4)_3$ structure but as our data does not show any weak low angle peaks to support a unit-cell volume doubling on transition similar to those seen for $Sc_2(WO_4)_3$ on transformation under pressure,[41] we have chosen to use the lower volume unit cell from our initial indexing. This choice has no impact on our determination of bulk moduli and subsequent discussion. This first monoclinic phase has a bulk modulus, K_0 =17(1) GPa, that is essentially identical to those for low-pressure monoclinic $Sc_2(MoO_4)_3$ and $Sc_2(WO_4)_3$, 16(1) and 14(1) GPa, respectively,[24,41] but much less than that for monoclinic $Al_2(WO_4)_3$,[24] K_0=28(1) GPa. All of these compounds display a reduction in bulk modulus on going through the orthorhombic-to-monoclinic phase transition. Similar behavior has previously been reported for materials with a ReO_3-type structure.[65] This structural family also has many of the features typical of NTE phases (open flexible frameworks with two-coordinate anions), although none of

TABLE IV. Phase-transition pressures and parameters from fitting third-order Birch-Murnaghan EoSs to the *P-V* data for $Zr_2(WO_4)(PO_4)_2$ shown in Tables I and II. In each case, K_p was fixed at 4 during the fit to the EoS.

		Run 1 compression	Run 1 decompression	Run 2 compression
Ortho	*P* range (GPa)	0.0–1.37	1.02–0.08	0.44–1.2
	V_0 (Å^3)	1058(1)	1053(1)	1062(2)
	K_0 (GPa)	49(2)	50(3)	48(5)
	Average *K* (GPa)	52	52	52
Mono 1	*P* range (GPa)	1.68–3.41	2.88–1.68	1.95–2.97[a]
	V_0 (Å^3)	1104(5)	1096(10)	1071(10)
	K_0 (GPa)	17(1)	17(2)	27(4)
	Average *K* (GPa)	27	26	37
Mono 2	*P* range (GPa)	3.87–5.35	5.27–3.32	3.7–6.3[b]
	V_0 (Å^3)	956(9)	954(3)	921(10)
	K_0 (GPa)	36(4)	37(1)	66(12)
	Average *K* (GPa)	55	53	89
Triclinic	*P* range (GPa)			7.41–13.76
	V_0 (Å^3)			885(8)
	K_0 (GPa)			76(7)
	Average *K* (GPa)			119

[a]Only four diffraction patterns were recorded in this range, leading to large estimated standard deviations (esds) for V_0 and K_0.

[b]Only four diffraction patterns were recorded in this range and two of them displayed phase coexistence reducing the accuracy of the lattice-constant determination, leading to large esds for both V_0 and K_0.

the compounds that have been closely examined [ReO_3,[66] TaO_2F,[67] and NbO_2F (Ref. 67)] display strong NTE. This initial monoclinic $Zr_2(WO_4)(PO_4)_2$ structure displays highly anisotropic compressibility ($\beta_c \sim 10 \times \beta_a$) whereas the other examined $A_2(MO_4)_3$-type monoclinic phases[24,41] show almost isotropic behavior. Structural studies of this $Zr_2(WO_4)(PO_4)_2$ phase are needed to help explain the origin of these differences.

The second monoclinic phase observed on compression of $Zr_2(WO_4)(PO_4)_2$ to greater than ~3 GPa is apparently similar in structure to the phases that were previously observed on compression of $Sc_2(WO_4)_3$ and $Sc_2(MoO_4)_3$ to greater than ~2.8 and ~2.5 GPa, respectively, and presumably similar to the phase reported to form on compressing $Sc_2(WO_4)_3$ to >1.6 GPa by Garg *et al.*[37] While we were unable to index the diffraction data for $Sc_2(WO_4)_3$ at the time of our earlier work,[41] a unit cell derived from the one proposed for $Zr_2(WO_4)(PO_4)_2$ also satisfactorily explains the high-pressure $Sc_2(WO_4)_3$ data. This second monoclinic phase for $Zr_2(WO_4)(PO_4)_2$ has a ~8% smaller volume per f.u. than the lower pressure monoclinic phase that it forms from at ~3 GPa. Phase coexistence was observed consistent with the discontinuous nature of the transition. The bulk modulus of this phase [K_0=37(1) GPa] is similar to that of the starting orthorhombic material and it shows anisotropic compressibility with the *a* axis expanding during compression. Surprisingly, this is much lower than the bulk modulus for the apparently analogous phase of $Sc_2(WO_4)_3$ (~90 GPa).[63]

At >6.3 GPa a further crystalline phase formed. This apparently triclinic material has an estimated bulk modulus, $K_0 \sim 76(7)$ GPa, greater than that of the starting orthorhombic phase. As far as we are aware, it is not structurally related to any previously seen $A_2(MO_4)_3$-type phases. This difference in behavior could arise from the substitution of phosphorous for tungsten. At high pressures, densification and phase transformations can involve increases in coordination number, for example, on modest compression of the NTE phase cubic ZrW_2O_8, an orthorhombic phase containing some tungsten sites with additional W-O bonding contacts is formed.[13] However, the replacement of tungsten with phosphorous, in a $A_2(MO_4)_3$-type structure, shuts off potential densification pathways that involve an increase in coordination number for the sites where substitution had occurred, as phosphorous in oxides does not readily adopt coordination numbers above 4,[68,69] unlike tungsten. Structure determination and confirmation of the proposed unit cell require better quality diffraction data. In particular, a larger sample-to-detector distance than could be used with the Mar345 detector at the CHESS B2 station would be beneficial.

The pressure-induced amorphization seen at >14 GPa for $Zr_2(WO_4)(PO_4)_2$ occurs in a regimen where the pressure

TABLE V. Summary of the characteristics for $Sc_2(WO_4)_3$ related materials at high pressure. K_0 and P_T denote the bulk modulus and phase-transition pressure, respectively. NF indicates that this phase is either not formed or has not been identified.

		$Sc_2(WO_4)_3$	$Sc_2(MoO_4)_3$	$Al_2(WO_4)_3$	$Y_2(WO_4)_3$	$Zr_2(WO_4)(PO_4)_2$
Ortho		*Pnca*	*Pnca*	*Pnca*	*Pnca*	*Pnca*
	K_0 (GPa)	31(3)[a]	32(2)[b]; 6[c]	48[b]	25[d]	49(2)
	P_T (GPa)	0.3[a]; 0.6[e]	0.29[f]	0.1[b]; 0.28[g]	4[d]	1.4
			0.25–0.6[b]	0.5[h]	disorders	
Mono 1		$P2_1/a$	$P2_1/a$	$P2_1/a$	NF	$P2_1/n$
	K_0 (GPa)	14(1)[a]	16(1)[b]	28(1)[b]		17(1)
	P_T (GPa)	2.8[a]; 1.6[e]	2.5–3[b]; 2.7[f]			3.4
Mono 2		$P2_1/n$	$AsSc_2(WO_4)_3$	NF	NF	$P2_1/n$
	K_0 (GPa)	90(3)[i]				37(1)
	P_T (GPa)	2.7				6.3
Triclinic						*P*1 or *P*-1
	K_0 (GPa)	NF	NF	NF	NF	76(7)
	P_T (GPa)					

[a]Reference 41.
[b]Reference 24.
[c]Reference 39.
[d]Reference 60.
[e]Reference 37.
[f]Reference 40.
[g]Reference 61.
[h]Reference 62.
[i]Reference 63.

transmitting medium is expected to be nonhydrostatic.[49] Pressure-induced amorphization in NTE materials is a common phenomenon that has received considerable discussion including the possibility that it is somehow related to NTE.[15] Its occurrence can be dependent on the stress state of the sample.[70–72] An amorphization pressure of ~14 GPa is high when compared to well-studied NTE oxides such as ZrW_2O_8 (1.5–3.5 GPa), $ZrMo_2O_8$ (<4 GPa), and ZrV_2O_7 (~4 GPa).[73,74] However, other members of the $Sc_2W_3O_{12}$ family of NTE materials undergo amorphization at pressures closer to that observed for $Zr_2(WO_4)(PO_4)_2$, $Sc_2(WO_4)_3$ [>10, ~14 GPa (Refs. 37 and 41)], $Sc_2(MoO_4)_3$ (~8 GPa) (Ref. 24), $Al_2(WO_4)_3$ [~14, >6 GPa (Refs. 24 and 75, respectively)], $Ga_2(MoO_4)_3$ (>8 GPa) (Ref. 76), and $Y_2(WO_4)_3$ (>4 GPa) (Ref. 60). It is possible that the replacement of tungsten by phosphorous shuts off amorphization pathways that involve an increase in coordination number for the tungsten and, hence, changes the conditions required for amorphization.

V. CONCLUSIONS

The high-pressure behavior of $Zr_2(WO_4)(PO_4)_2$ is quite different from that reported for $A_2(MO_4)_3$ phases (A=+3 ion, M=W or Mo) that adopt a $Sc_2(WO_4)_3$ structure under ambient conditions. Three crystalline-to-crystalline phase transitions were observed followed by irreversible amorphization at >14 GPa. The first phase transition, leading to a loss of the orthorhombic $Sc_2(WO_4)_3$ structure that is associated with negative thermal expansion, occurred at much higher pressure (~1.4 GPa) than has been seen for related materials (<0.5 GPa). The first high-pressure phase that is formed may have a different structure from that seen in a previous work on $A_2(MO_4)_3$. The second high-pressure phase formed on compression of $Zr_2(WO_4)(PO_4)_2$ is probably structurally related to the high-pressure form of $Sc_2(WO_4)_3$ seen at ~3 GPa. An additional crystalline high-pressure phase is formed at >6.3 GPa.

ACKNOWLEDGMENTS

This work is based on experiments conducted at the Cornell High Energy Synchrotron Source (CHESS), which is supported by the National Science Foundation and the National Institutes of Health/National Institute of General Medical Sciences under Grant No. DMR-0225180. A.P.W. is grateful for support under National Science Foundation Grants DMR-0203342 and DMR-0605671. We are grateful for experimental assistance while at CHESS from C.-S. Zha.

*FAX: 404 894 7452; angus.wilkinson@chemistry.gatech.edu

[1] A. W. Sleight, Endeavour **19**, 64 (1995).
[2] A. W. Sleight, Inorg. Chem. **37**, 2854 (1998).
[3] A. W. Sleight, Annu. Rev. Mater. Sci. **28**, 29 (1998).
[4] A. W. Sleight, Curr. Opin. Solid State Mater. Sci. **3**, 128 (1998).
[5] J. S. O. Evans, T. A. Mary, and A. W. Sleight, Physica B **241-243**, 311 (1997).
[6] J. S. O. Evans, J. Chem. Soc. Dalton Trans. **1999**, 3317.
[7] J. S. O. Evans, T. A. Mary, and A. W. Sleight, J. Solid State Chem. **133**, 580 (1997).
[8] E. Breval and D. K. Agrawal, Br. Ceram. Trans. **94**, 27 (1995).
[9] R. Roy, D. K. Agrawal, and H. A. McKinstry, Annu. Rev. Mater. Sci. **19**, 59 (1989).
[10] G. E. Lenain, H. A. McKinstry, J. Alamo, and D. K. Agrawal, J. Mater. Sci. **22**, 17 (1987).
[11] D. A. Woodcock, P. Lightfoot, and C. Ritter, Chem. Commun. (Cambridge) **1998**, 107.
[12] D. A. Woodcock, P. Lightfoot, and R. I. Smith, J. Mater. Chem. **9**, 2631 (1999).
[13] J. S. O. Evans, Z. Hu, J. D. Jorgensen, D. N. Argyriou, S. Short, and A. W. Sleight, Science **275**, 61 (1997).
[14] T. A. Mary, J. S. O. Evans, T. Vogt, and A. W. Sleight, Science **272**, 90 (1996).
[15] C. A. Perottoni and J. A. H. de Jornada, Science **280**, 886 (1998).
[16] V. Korthuis, N. Khosrovani, A. W. Sleight, N. Roberts, R. Dupree, and W. W. Warren, Chem. Mater. **7**, 412 (1995).
[17] Robert C. Wetherhold and Jianzhong Wang, Compos. Sci. Technol. **53**, 1 (1995).
[18] D. A. Fleming, D. W. Johnson, and P. J. Lemaire, U.S. Patent No. 5,694,503 (1997).
[19] D. A. Fleming, P. J. Lemaire, and D. W. Johnson, European Patent No. EP 0,828,169 (A2) (1998).
[20] D. K. Balch and D. C. Dunand, Metall. Mater. Trans. A **35A**, 1159 (2004).
[21] A. Grzechnik and W. A. Crichton, Solid State Sci. **4**, 1137 (2002).
[22] D. V. S. Muthu, B. Chen, J. M. Wrobel, A. M. Krogh Andersen, S. Carlson, and M. B. Kruger, Phys. Rev. B **65**, 064101 (2002).
[23] J. D. Jorgensen, Z. Hu, S. Short, A. W. Sleight, and J. S. O. Evans, J. Appl. Phys. **89**, 3184 (2001).
[24] T. Varga, A. P. Wilkinson, C. Lind, W. A. Bassett, and C.-S. Zha, J. Phys.: Condens. Matter **17**, 4271 (2005).
[25] B. Chen, D. V. S. Muthu, Z. X. Liu, A. W. Sleight, and M. B. Kruger, Phys. Rev. B **64**, 214111 (2001).
[26] T. Varga, A. P. Wilkinson, A. C. Jupe, C. Lind, W. A. Bassett, and C.-S. Zha, Phys. Rev. B **72**, 024117 (2005).
[27] T. Varga, A. P. Wilkinson, C. Lind, W. A. Basset, and C.-S. Zha, Solid State Commun. **135**, 739 (2005).
[28] R. A. Secco, H. Liu, N. Imanaka, and G. Adachi, J. Mater. Sci. Lett. **20**, 1339 (2001).
[29] H. Holzer and D. C. Dunand, J. Mater. Res. **14**, 780 (1999).
[30] S. Yilmaz, J. Phys.: Condens. Matter **14**, 365 (2002).
[31] K. Nassau, H. J. Levinstein, and G. M. Loiacono, J. Am. Ceram. Soc. **47**, 363 (1964).
[32] K. Nassau, H. J. Levinstein, and G. M. Loiacono, J. Phys. Chem. Solids **26**, 1805 (1965).
[33] S. C. Abrahams and J. L. Bernstein, J. Chem. Phys. **45**, 2745 (1966).
[34] A. W. Sleight and L. H. Brixner, J. Solid State Chem. **7**, 172 (1973).
[35] J. S. O. Evans and T. A. Mary, Int. J. Inorg. Mater. **2**, 143 (2000).
[36] A. K. Tyagi, S. N. Achary, and M. D. Mathews, J. Alloys Compd. **339**, 207 (2002).
[37] N. Garg, C. Murli, A. K. Tyagi, and S. M. Sharma, Phys. Rev. B **72**, 064106 (2005).
[38] A. K. Arora, R. Nithya, T. Yagi, N. Miyajima, and T. A. Mary, Solid State Commun. **129**, 9 (2004).
[39] A. K. Arora, T. Yagi, N. Miyajima, and T. A. Mary, J. Appl. Phys. **97**, 013508 (2005).
[40] W. Paraguassu, M. Maczka, A. G. Souza Filho, P. T. C. Freire, J. Mendes Filho, F. E. A. Melo, L. Macalik, L. Gerward, J. Staun Olsen, A. Waskowska, and J. Hanuza, Phys. Rev. B **69**, 094111 (2004).
[41] T. Varga, A. P. Wilkinson, C. Lind, W. A. Bassett, and C.-S. Zha, Phys. Rev. B **71**, 214106 (2005).
[42] A. M. Gindhart, C. Lind, and M. Green, J. Mater. Res. **23**, 210 (2008).
[43] T. Suzuki and A. Omote, J. Am. Ceram. Soc. **87**, 1365 (2004).
[44] C. A. Martinek and F. A. Hummel, J. Am. Ceram. Soc. **53**, 159 (1970).
[45] A. N. Tsvigunov and V. P. Sirotinkin, Russ. J. Inorg. Chem. **35**, 1740 (1990).
[46] J. S. O. Evans, T. A. Mary, and A. W. Sleight, J. Solid State Chem. **120**, 101 (1995).
[47] V. P. Sirotinkin and A. N. Tsvigunov, Russ. J. Inorg. Chem. **39**, 735 (1994).
[48] M. Cetinkol and A. P. Wilkinson, Solid State Commun. **149**, 421 (2009).
[49] G. J. Piermarini, S. Block, and J. D. Barnett, J. Appl. Phys. **44**, 5377 (1973).
[50] M. Cetinkol, A. P. Wilkinson, C. Lind, W. A. Bassett, and C.-S. Zha, J. Phys. Chem. Solids **68**, 611 (2007).
[51] J. D. Barnett, S. Block, and G. J. Piermarini, Rev. Sci. Instrum. **44**, 1 (1973).
[52] A. P. Hammersley, S. O. Svensson, M. Hanfland, A. N. Fitch, and D. Hausermann, High Press. Res. **14**, 235 (1996).
[53] Computer code JADE, Materials Data, Inc., Livermore, CA, 1995–2005.
[54] P. E. Werner, L. Eriksson, and M. Westdahl, J. Appl. Crystallogr. **18**, 367 (1985).
[55] B. H. Toby, J. Appl. Crystallogr. **38**, 1040 (2005).
[56] A. C. Larson and R. B. Von Dreele, General Structure Analysis System (GSAS), Los Alamos Laboratory Report No. LA-UR-86-748, 1987.
[57] B. H. Toby, J. Appl. Crystallogr. **34**, 210 (2001).
[58] F. Birch, Phys. Rev. **71**, 809 (1947).
[59] R. J. Angel, computer code EOS-FIT, Virginia Tech, Blacksburg, VA, 2001.
[60] S. Karmakar, S. K. Deb, A. K. Tyagi, and S. M. Sharma, J. Solid State Chem. **177**, 4087 (2004).
[61] M. Maczka, W. Paraguassu, A. G. Souza Filho, P. T. C. Freire, J. Mendes Filho, F. E. A. Melo, and J. Hanuza, J. Solid State Chem. **177**, 2002 (2004).
[62] G. D. Mukherjee, V. Vijaykumar, S. N. Achary, A. K. Tyagi, and B. K. Godwal, J. Phys.: Condens. Matter **16**, 7321 (2004).
[63] M. Cetinkol, A. P. Wilkinson, and K. W. Chapman, Solid State Commun. **148**, 511 (2008).
[64] S. Sumithra and A. M. Umarji, Mater. Res. Bull. **40**, 167 (2005).

[65] J. E. Schirber and B. Morosin, Phys. Rev. Lett. **42**, 1485 (1979).
[66] D. Taylor, Br. Ceram. Trans. J. **84**, 9 (1985).
[67] J. Z. Tao and A. W. Sleight, J. Solid State Chem. **173**, 45 (2003).
[68] J. Pellicer-Porres, A. M. Saitta, A. Polian, J. P. Itie, and M. Hanfland, Nature Mater. **6**, 698 (2007).
[69] M. A. Salvado and P. Pertierra, Inorg. Chem. **47**, 4884 (2008).
[70] S. M. Sharma and S. K. Sikka, Prog. Mater. Sci. **40**, 1 (1996).
[71] C. Lind, D. G. VanDerveer, A. P. Wilkinson, J. Chen, M. T. Vaughan, and D. J. Weidner, Chem. Mater. **13**, 487 (2001).
[72] K. J. Kingma, C. Meade, R. J. Hemley, H. K. Mao, and D. R. Veblen, Science **259**, 666 (1993).
[73] S. Carlson and A. M. Krogh Andersen, J. Appl. Crystallogr. **34**, 7 (2001).
[74] T. Sakuntala, A. K. Arora, V. Sivasubramanian, R. Rao, S. Kalavathi, and S. K. Deb, Phys. Rev. B **75**, 174119 (2007).
[75] N. Garg, V. Panchal, A. K. Tyagi, and S. M. Sharma, J. Solid State Chem. **178**, 998 (2005).
[76] S. D. Gates, J. A. Colin, and C. Lind, J. Mater. Chem. **16**, 4214 (2006).